Silicon (2021) 13:3399–3412
https://doi.org/10.1007/s12633-020-00751-4

ORIGINAL PAPER

Performance Analysis of Nano Silicon Carbide Reinforced Swept Friction Stir Spot Weld Joint in AA6061-T6 Alloy

S. Suresh[1] · K. Venkatesan[2] · Elango Natarajan[3] · S. Rajesh[4]

Received: 29 July 2020 / Accepted: 1 October 2020 / Published online: 30 October 2020

Abstract

Swept friction stir spot welding (SFSSW) is one of the preferred welding methods used in joining metals. The application of this joining process is limited by path deviation, insufficient tool plunging and vibrations caused by high torque and force during the welding. In order to improve the weld strength and weld repeatability, the optimum process parameters of SFSSW of aluminium 6061-T6 alloy were investigated through Grey rational analysis. Initially, Taguchi L_{16} array consisting of diameter of guide hole, tool rotational and traverse speeds was developed and experiments were conducted by filling guide hole with Silicon Carbide nanoparticles. Grey relational analysis of the experiments reports that guide hole diameter = 3 mm, rotational speed = 1600 rpm and traverse speed = 20 mm/min are found to be optimal parameters for attaining the maximum lap shear strength and hardness. The cause-and-effect analysis of data reports that the amount of SiC added to the guide hole is the most significant factor influencing the weld strength. Furthermore, mechanical and metallurgical characterisation of weld samples prepared at optimum condition were compared with neat samples. The microstructural analysis of stir zone and the fractured area were also presented. The addition of nanoparticles and use of predicted optimum weld condition results homogeneous distribution, refined grains in the stir zone that causes a noteworthy increase in the weld strength.

Keywords Swept friction stir spot welding · SiC nanoparticles · Multi-response optimization · Grey relational analysis · Lap shear strength · Microhardness

1 Introduction

The exclusive and excellent physical, mechanical and tribological properties of aluminium and its alloys have made them to be the predominant material in industrial applications. Aluminium alloys and aluminium composites have set a benchmark in achieving reduced weight and improved fuel efficiency in transport. The aluminiumsheetsare commonly used in automotive panels, aircraft and ship structure building [1]. Aluminium 6xxx finds its use in automobile due to its better weldability and improved strength-to-weight ratio. It is implied for better fuel economy among the existing different series of aluminium alloys [2]. Friction stir spot welding (FSSW) is sustainable solid-state welding preferred for joining sheet metals. It is particularly applied for aluminium alloys in the last few decades to overcome the issues that arise in fusion welding and other joining processes [3]. Unlike the other welding processes where the base material is melted, FSSW uses a non-consumable rotating tool to produce the joints. The process sequence of conventional FSSW consists of plunging, dwelling and retraction motions of the tool [4]. The variants of FSSW are; (i) Swept FSSW [5] (ii) The refill FSSW [6] (iii) Swing FSSW and Stitch FSSW [7, 8]. The swept FSSW was further modified at Wichita State University, named as Octospot FSSW [9]. Swept FSSW produces the weld by the plunge and translation of a rotating tool around a circular or elliptical path around the exit hole.

Some of the researches on conventional FSSW relating to improvement of mechanical strength and analysis of process parameters can be found in [10–15]. There are only a

✉ S. Suresh
suresh.mjl@gmail.com

[1] Department of Mechanical Engineering, Jayalakshmi Institute of Technology, Thoppur, India

[2] Department of Metallurgical Engineering, Government College of Engineering, Salem, India

[3] Faculty of Engineering, UCSI University, Kuala Lumpur, Malaysia

[4] Department of Mechanical Engineering, Knowledge Institute of Technology, Salem, India

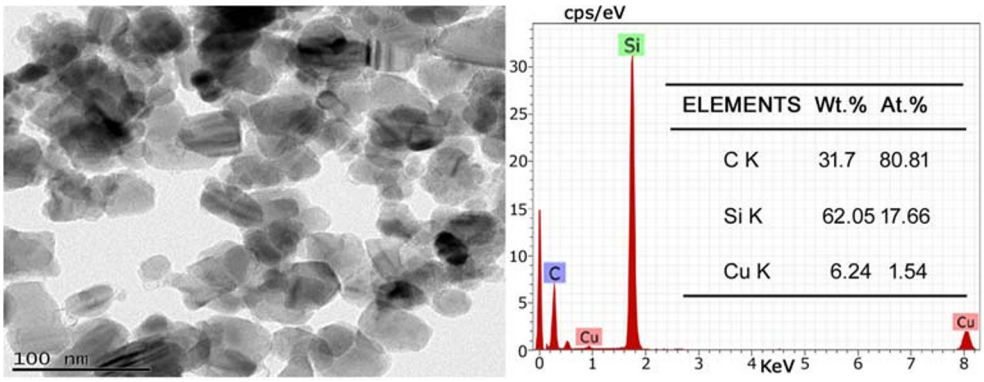

Fig. 1. TEM micrograph with EDS analysis of SiC nanoparticles

very few literatures found on swept FSSW process compared to conventional FSSW to the knowledge of authors. Su et al. [16, 17] used the swept FSSW process to evaluate the fatigue life of corrosion-resistant aluminium alloy and reported that the circular motion of tool affects the fatigue life of joints. The fabrication of FSSW nanocomposite joint is geared up in recent years. The friction stir welding and friction stir processing of aluminium alloy with the addition of ceramic particles like SiC, B_4C, TiB_2, WC and Al_2O_3 to enhance the physical, mechanical and tribological properties were reported in [18–21]. The addition of SiC particles showed better weld strength than other fillers due to their lower thermal expansion coefficient, excellent coherency with the metal matrix. Suresh et al. [22] reported the benefit of the reinforcement of SiC nanoparticles in conventional FSSW of 6061-T6 aluminium alloy. Wu et al. [23] conducted the FSSW experiments on AZ31 magnesium alloy with addition of SiC particles in the weld regions and reported that both the lap shear strength and microhardness of welds were found to increase by grain boundary strengthening. Tebyani et al. [24] used SiC nanoparticles of 25 nm in size to fabricate interstitial-free steel FSSW joint and reported that the hardness and joint strength were significantly improved compared to SiC free FSSW. These above researches have particularly focused on the enhancement of mechanical property and metallurgical behaviour of the welds.

The effective optimization of weld condition is desirable to produce welds with stability of quality response. The single response optimization was previously conducted in [25–27]. Ojo and Taban [28] used multi-objective optimization on FSSW of AA2219-O alloy and reported the effect of welding parameters on shear load, bonded size and flash volume.

Understanding that only a limited research has been conducted on multi-objective optimization of FSSW, more particularly on swept FSSW joints on aluminium alloys, the current research is aimed to determine optimal weld condition to produce high weld strength on 6061-T6 aluminium alloy.

Taguchi grey relational analysis (GRA) is a straightforward and accurate method for selecting influential parameters in multi-output systems with unique characteristics, that proven by many researches especially in materials processing [29–31]. In the present study, authors initially developed design of experiments (DOE) with four levels of each control parameter and conducted the experiments to measure the response variables for each set of control parameters. Secondly, GRA was applied to optimize the process parameters with multi-response features of the joints. The results of GRA was further validated experimentally. Lastly, microstructural analysis of

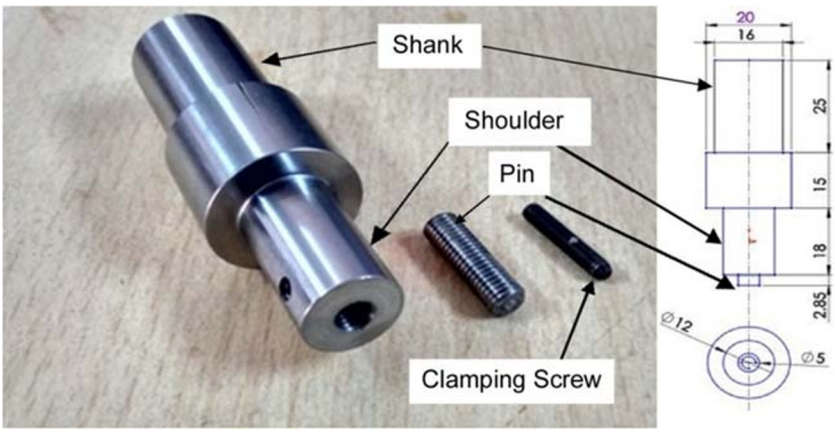

Fig. 2 SFSSW tool and its dimensions (All the dimensions are in mm)

weld regions and fractured samples produced under optimum conditions were conducted to understand the distribution of nanoparticles and failure mechanism.

2 Experimental Method

2.1 Materials

Mg-based Al alloy, known as AA6061-T6was the material chosen for the current research as it is mostly used in automobile frames and structures. The constituents of the chosen base metal are 0.708% Mg, 0.43% Si, 0.49% Fe, 0.164% Cu, 0.14% Cr, 0.097% Mn, 0.04% Ti, 0.004% Zn and the rest wt% of Al. The weld test coupons ofAA6061-T6 in the size of 100 × 35 × 2 mm was firstly prepared using electrical discharge machine (EDM). The samples were then cleaned using acetone. The average size of 50 nm SiC nanoparticles (received from Hongwu International Group Ltd., Hong Kong) were used for the reinforcement. The sufficient amount of nanoparticles was reinforced in the weld area through the guide hole that appears on the top sheet and at the centre of the overlap area. Figure 1 shows transmission electron micrograph and elemental description of SiC nanoparticle (as received from the supplier). The tool used was of H13 grade steel with hardness of 56–60 HRC. Figure 2 shows the dimensions and the photograph of the tool used for Swept Friction Stir Spot Welding (SFSSW).

2.2 Design of Experiments (DOE)

Taguchi orthogonal array (OA) was espoused to design the number of experiments to be conducted. Guide hole diameter (mm) where nanoparticles are reinforced, tool rotational speed (rpm) and tool traverse speed (mm/min) were chosen as independent variables (process parameters), while microhardness and lap shear strength were response variables. To identify the levels of each process parameter for DOE, different values of guide hole, rotational and traverse speed of tool were used to conduct the preliminary experiments. From the preliminary experiments, the following were arrived;

(1) No significant effect of SiC reinforcement observed up to 1.5 mm diameter of guide hole. Moreover, packed nanoparticle was started spill out from the guide hole during plunging of the tool, when the diameter is more than 3 mm. Hence, the guide hole diameter must be between 1.5 mm and 3 mm.
(2) Surface defects were observed up to 1200 rpm of tool rotational speed. Also, joint was not established when it is more than 1800 rpm.
(3) Surface defect and tunnel defects were observed when tool traverse speed was less than 10 mm/min and more than 25 mm/min.

Table 1 Process parameters of SFSSW and their levels

Process parameters	Symbol	Levels			
		1	2	3	4
Guide hole diameter (mm)	D	1.5	2	2.5	3
Tool rotational speed (rpm)	N	1200	1400	1600	1800
Tool traverse speed (mm/min)	F	10	15	20	25

The levels of weld parameters as shown in Table 1 were based on the preliminary experiments, previous research and the literatures [25, 32–34, and]. The welding according to L_{16} orthogonal array shown in Table 2 was carried out in a CNC vertical machining centre that has a special fixture for clamping the overlapping area of the base material as shown in Fig. 3. Three weld samples at each set of process parameters were prepared. The respective response variables such as microhardness and lap shear strength were measured for each sample. The photograph of weld samples used for lap shear test and setup of lap shear test were shown in Fig. 4(a) and (b), respectively.

2.3 Mechanical Tests and Characterisation of Weld Cross-Sections

The microhardness test was done with 1 kg of force for a dwell time of 20 s using Vicker's microhardness tester (Wilson hardness, 402 MVD). The readings were taken at four different locations of the weld area of each sample and the mean of the

Table 2 L_{16} Orthogonal array of process parameters

Exp No.	Guide hole diameter (D) in mm	Tool rotational speed (N) in rpm	Tool traverse speed (F) in mm/min
1	1.5	1200	10
2	1.5	1400	15
3	1.5	1600	20
4	1.5	1800	25
5	2.0	1200	15
6	2.0	1400	10
7	2.0	1600	25
8	2.0	1800	20
9	2.5	1200	20
10	2.5	1400	25
11	2.5	1600	10
12	2.5	1800	15
13	3.0	1200	25
14	3.0	1400	20
15	3.0	1600	15
16	3.0	1800	10

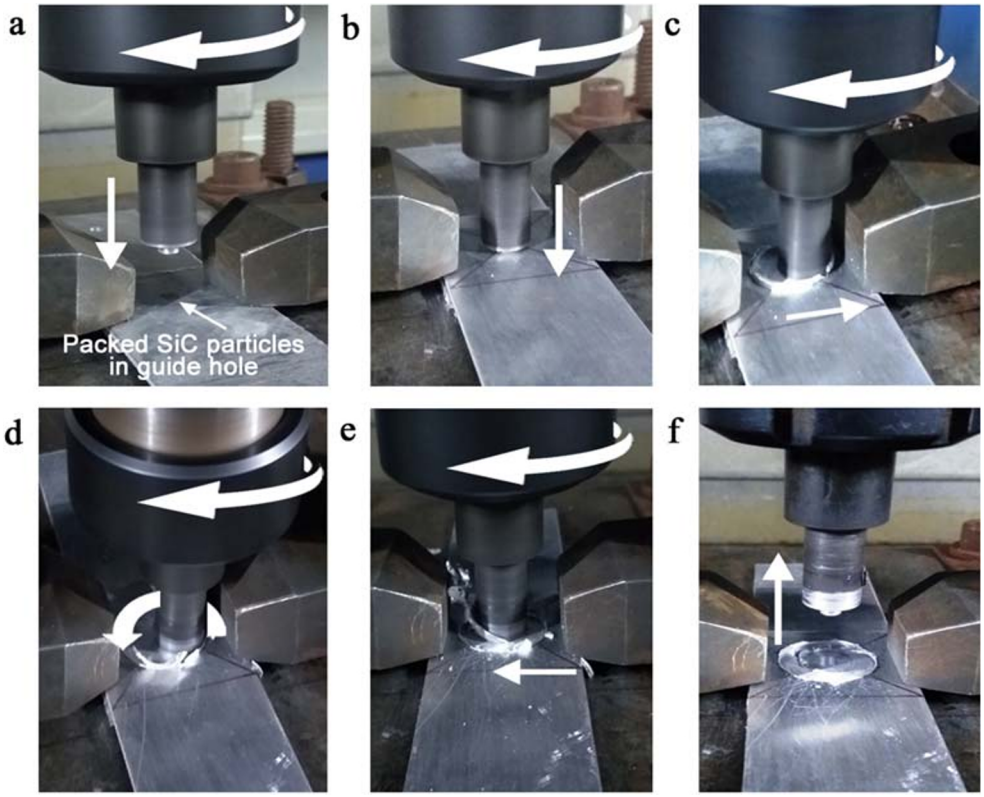

Fig. 3 SFSSW conducted: (**a**) Packed SiC particles in guide hole (**b**) The rotating tool plunging into the overlapped plates creating heat and stirring (**c**) Linear movement of the tool (**d**) Tool travelling 360^0circular sweeping (**e**) Linear movement of the tool to weld centre (**f**) Retraction of the tool from the joint

readings was recorded. In the same way, three samples were examined to ensure the repeatability of the measured values.

Computerized Universal Testing Machine (model: TE-JINAN-WDW100) was used to conduct the lap shear tensile test on the as-welded samples at the room temperature. The sample was attached to a gripper and the load was applied at 1 mm/min till the sample fractures. The respective shear load of the sample was noticed.

To observe the macro and microstructures, the weld samples were initially cross-sectioned at the tool plunge centre. The cross-sectioned samples were then etched with Keller's reagent (5 ml HNO_3, 3 ml HCl, 2 ml HF and 190 ml H_2O) to study the microstructure. The macrostructure of the cross-sectioned sample was investigated using stereo zoom microscope (model: Radical RSM - 9). The microstructure characterization of the cross-section of the joints were investigated

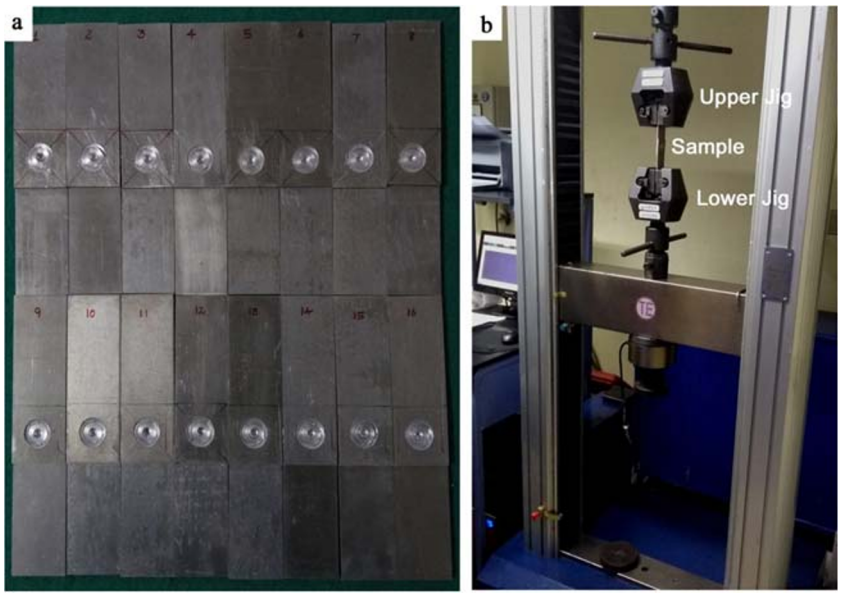

Fig. 4 (**a**) Fabricated SFSSW samples for lap shear test (**b**) Lap shear test setup

through optical microscope (model: Invertoplan TR). The distribution of nanoparticles in the weld area and mechanism of fracture of lap shear tested specimens were studied through field emission scanning electron microscope (model: SIGMA - Carl Zeiss with Xflash 5030 detector).

3 Results and Discussions

3.1 Experimental Results and S/N Ratios

In Taguchi method, the logarithmic transformation of the responses is called signal-to-noise (S/N) ratio. It is calculated using the larger-the-better criterion.

$$S/_N = -10 \log_{10} \frac{1}{n} \sum_{i=1}^{n} \left(\frac{1}{y_i^2} \right) \quad (1)$$

Here y_i and n are represented observed response and the number of observations, respectively. Table 3 shows all experimental data and their respective S/N ratios.

3.2 Multi-Response Optimization Using Gray Rational Analysis (GRA)

GRA is one of the effective system analysis tools. It makes a base for modelling, clustering, and forecasting of grey systems. It has many advantages such as accurate method for selecting factors, small sample and no requirement for independence. The computed S/N ratio of microhardness and lap shear strength shown in Table 3 were used as input data for GRA multi-response optimization. The below sections detail the methodology and results of multi-response optimization.

Table 3 Measured response variables and the respected signal to noise ratio (S/N)

Exp No.	Response variables		S/N ratio	
	Microhardness (HV)	Lap shear strength (N)	Microhardness (HV)	Lap shear strength (N)
1	88	5740	38.89	75.18
2	92	5954	39.28	75.50
3	94.4	6100	39.50	75.71
4	92.6	5976	39.33	75.53
5	92	5889	39.28	75.40
6	95.4	5999	39.59	75.56
7	97.4	6419	39.77	76.15
8	98.6	6412	39.88	76.14
9	98.5	6456	39.87	76.20
10	96.1	6427	39.65	76.16
11	99.6	6645	39.97	76.45
12	100.5	6654	40.04	76.46
13	99.8	6598	39.98	76.39
14	101.4	6987	40.12	76.89
15	104.6	6788	40.39	76.63
16	100	6620	40.00	76.42

Table 4 Computed grey relational generation and Deviational sequence

Exp No.	Grey relational generation		Deviation Sequence	
	Microhardness (HV)	Lap shear strength (N)	Microhardness (HV)	Lap shear strength (N)
1	0.000	0.000	1.000	1.000
2	0.252	0.186	0.748	0.814
3	0.397	0.309	0.603	0.691
4	0.288	0.205	0.712	0.795
5	0.252	0.130	0.748	0.870
6	0.457	0.224	0.543	0.776
7	0.575	0.569	0.425	0.431
8	0.644	0.563	0.356	0.437
9	0.638	0.598	0.362	0.402
10	0.499	0.575	0.501	0.425
11	0.701	0.745	0.299	0.255
12	0.752	0.752	0.248	0.248
13	0.712	0.709	0.288	0.291
14	0.802	1.000	0.198	0.000
15	0.978	0.853	0.022	0.147
16	0.724	0.726	0.276	0.274

Table 5 Predicted GRC and GRG

Exp No.	Grey Relational Coefficient		Grey Relational Grade (GRG)	Rank
	Microhardness (HV)	Lap shear strength (N)		
1	0.333	0.333	0.333	16
2	0.401	0.381	0.391	14
3	0.454	0.420	0.437	11
4	0.413	0.386	0.399	13
5	0.401	0.365	0.383	15
6	0.479	0.392	0.436	12
7	0.540	0.537	0.539	9
8	0.584	0.534	0.559	8
9	0.580	0.554	0.567	7
10	0.499	0.541	0.520	10
11	0.626	0.662	0.644	5
12	0.668	0.668	0.668	3
13	0.635	0.632	0.633	6
14	0.717	1.000	0.858	2
15	0.959	0.773	0.866	1
16	0.644	0.646	0.645	4

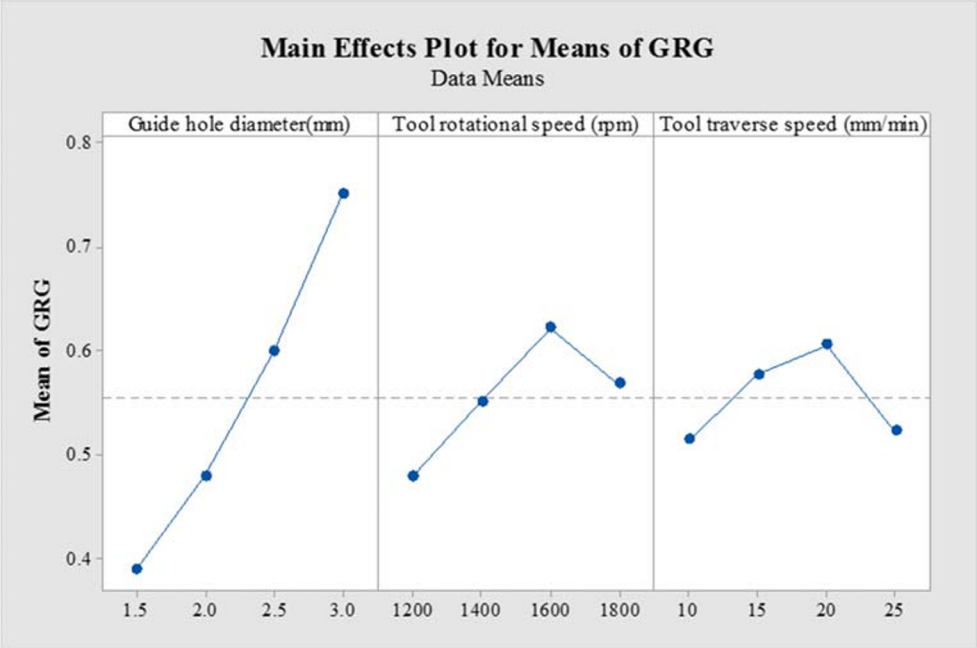

Fig. 5 Main effect plot for GRG

3.2.1 Grey-Relational Generation

Grey-Relational Generation (Normalization) is a pre-processing stage of GRA which converts all response values to the numbers in the range between 0 and 1. This method has different equations according to various quality characteristics; Smaller-the-best, Nominal-the-best and Larger-the-best. As the current research focuses on maximizing hardness and lap shear strength, the characteristic called "larger is better" was used. The normalised data and deviational sequences were calculated using Eqs. 2 and 3 respectively.

$$x_i^*(k) = \frac{X_i(k) - \min X_i(k)}{\max X_i(k) - \min X_i(k)} \tag{2}$$

$$\Delta_{0i}(K) = \left| X_0^*(K) - X_i^*(K) \right| \tag{3}$$

where X^*_i (k) and Δ_{0i} (k) are the sequences after the data normalization and deviational sequence respectively. Table 4 depicts the normalization and deviation sequences of the response variables.

3.2.2 Grey Relational Coefficient (GRC) and the Grey Relational Grade (GRG)

Grey Relational Coefficient (GRC) is a coefficient evaluated for each response. The weighted values of these coefficients are termed as Grey Relational Grade (GRG). It is distributed between 0 and 1 by averaging GRC. The GRC and GRG for each experiment of the L_{16} OA were calculated using Eqs. 4 and 5 and presented in Table 5.

$$\xi_i(K) = \frac{\Delta_{min} + \zeta\, \Delta_{max}}{\Delta_{0i}(k) + \zeta\, \Delta_{max}} \tag{4}$$

$$\gamma_i = \frac{1}{n} \sum_{i=1}^{n} \xi_i(K) \tag{5}$$

Where ξ is the identification coefficient whose value is taken as 0.5. It is noticed that Exp. No.15 has the highest GRG of 0.866 which regards to be the best predicted multi-response characteristic.

Figure 5 shows the main effect plot of GRG and Table 6 shows the response table of GRG for all input process parameters. It is found that the welding conditions under 3 mm guide hole diameter, 1600 rpm tool rotational speed and 20 mm/min tool traverse speed gives the optimum combination to have the maximum hardness and lap shear for AA6061-T6/SiC SFSSW joint. It is observed that, as the guide hole diameter increases, the multiple performance characteristics of the Al/SiC weld joints also

Table 6 Response table of GRG

Level	Guide hole diameter (mm)	Tool rotational speed (rpm)	Tool traverse speed (mm/min)
1	0.3910	0.4822	0.5183
2	0.4820	0.5550	0.5844
3	0.6052	0.6294	0.6105
4	0.7614	0.5730	0.5263
Delta	0.3704	0.1471	0.0923
Rank	1	2	3

Table 7 ANOVA table of grey relational grade

Source	DF	Adj SS	Adj MS	F-Value	*P* Value	% Contribution
Guide hole diameter (mm)	3	0.30908	0.103026	22.07	0.001	76.24%
Tool rotational speed (rpm)	3	0.04421	0.014738	3.16	0.107	10.90%
Tool traverse speed (mm/min)	3	0.02409	0.008030	1.72	0.262	5.94%
Error	6	0.02801	0.004668			
Total	15	0.40539				

Table 8 Confirmation test results

	Initial condition	Optimal Condition	
		Predicted by GRA	Validation Experiment
Parameter Level	D_1 N_1 F_1	D_4 N_3 F_3	D_4 N_3 F_3
Microhardness (HV)	88	–	105
Lap shear strength (N)	5740	–	6790
Gray relation grade (GRG)	0.333	0.881	0.887

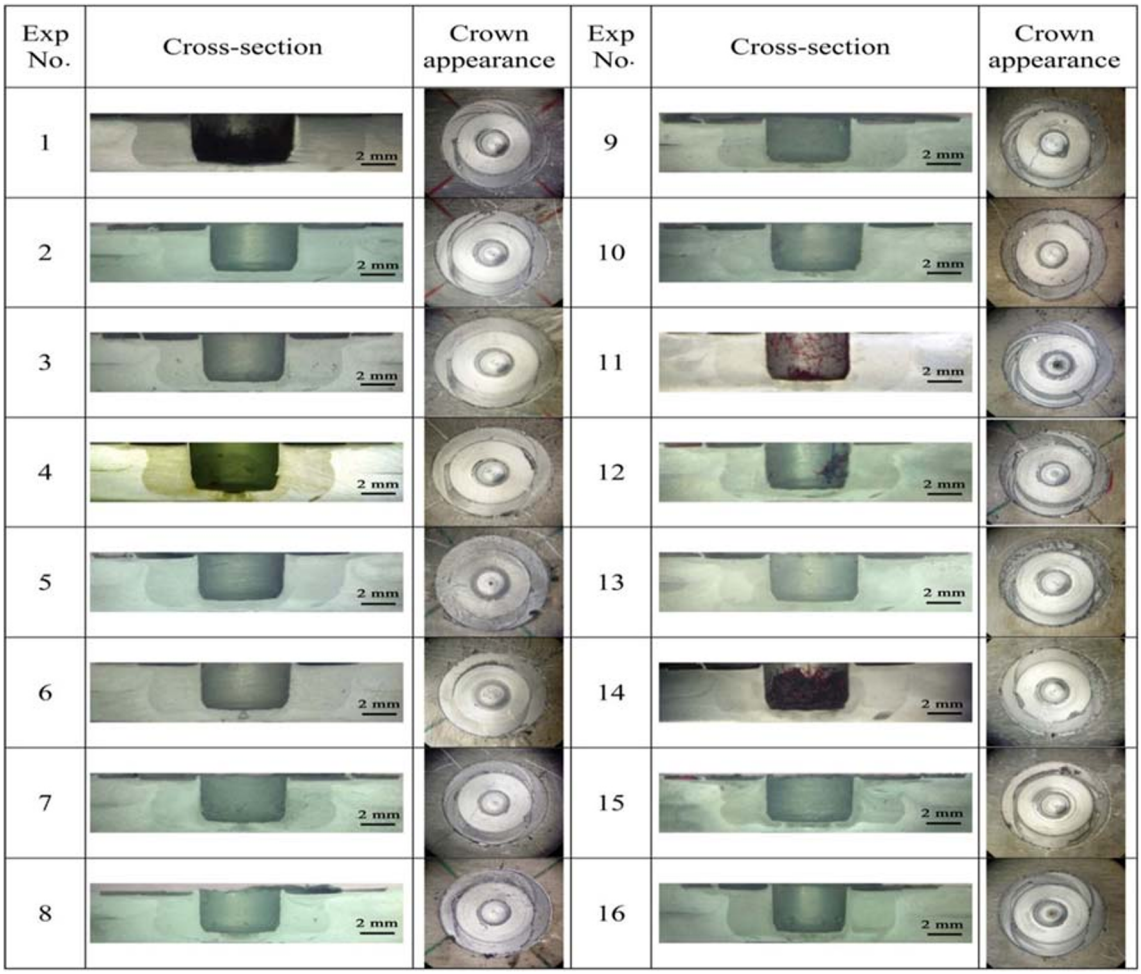

Fig. 6 Macrostructure and crown appearance of SFSSW joints

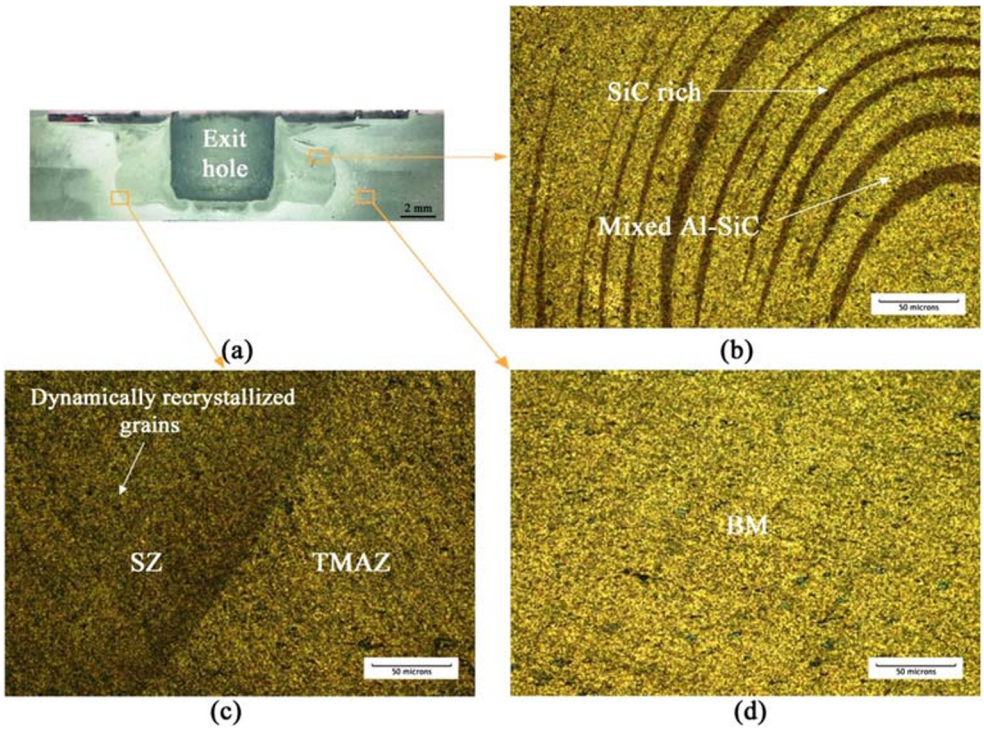

Fig. 7 (**a**) Macrograph of a cross-section of the weld fabricated under optimal parameters. And optical micrographs showing different regions of the joint: (**b**) Onion ring structure in SZ (**c**) Interface among SZ/TMAZ, and (**d**) BM

increases. Furthermore, when tool rotational speed and tool traverse speed increase, the multi-performance characteristic of the joints first increases to a maximum value up to a particular extent, then decreases with further enrichment.

3.3 Analysis of Variance (ANOVA) Study

The statically greater influence of independent variables on the multi responses was examined through ANOVA. The GRG data obtained from all the experiments were keyed into ANOVA tool and the analysis was done at 95% confidence level. Based on the results shown in Table 7, the guide hole diameter (amount of nanoparticles) appears to be the most significant parameter with 76.24% of contribution ($F = 22.07$, $p < 0.05$). This is followed by the tool rotational speed of 10.90% ($F = 3.16$) and the tool traverse speed of 5.94% ($F = 1.72$). It vividly evidences that the more amount of SiC nanoparticles used in the guide hole helps in getting high hardness and lap shear strength at the welded zone.

3.4 Confirmation Experiment and Results

In order to ensure the result of GRA, a confirmation experiment was carried out with optimal condition resulted by GRA. The optimum parameters; the guide hole diameter (D) = 3 mm, tool rotational speed (N) = 1600 rpm and the tool traverse speed (F) = 20 mm/min was used to prepare three weld samples. It is found from the validation experiments that the microhardness = 105 HV and lap shear strength = 6790 N and the corresponding GRG is 0.887. Table 8 shows a comparison between validation results and predicted results. The GRG of the sample prepared at the initial condition (the guide hole diameter (D) = 1.5 mm, tool rotational speed (N) = 1200 rpm and the tool traverse speed (F) = 10 mm/min) is 0.333.

The GRG of results from optimal condition is 62.46% higher than results from the initial level setting. It can be further inferred that the low percentage of error (0.681%) is noticed between the predicted GRG and the GRG of validation experiment. This shows the reliability and accuracy of the multi-objective optimization and the experimental work being carried out.

Improvement of grey relational grade between initial setting level to optimal setting level = 62.46%.

3.5 Weld Structure Characterization

The macrograph of cross-sectioned samples and the crown appearance of the weld joints prepared with different weld parameters are shown in Fig. 6. The similar crown appearance with no discontinuities is noticed in all weld joints. The cross-sectional macro appearance of the joint shows the observable Stir Zone (SZ). The images evidence the complete flow of plasticized material and formation of a composite joint during SFSSW. It is also observed that joints are free from defects such as tunnels, voids and cracks. The absence of defects evidences the good selection of welding parameters used in all sixteen experiments (according to L_{16} OA).

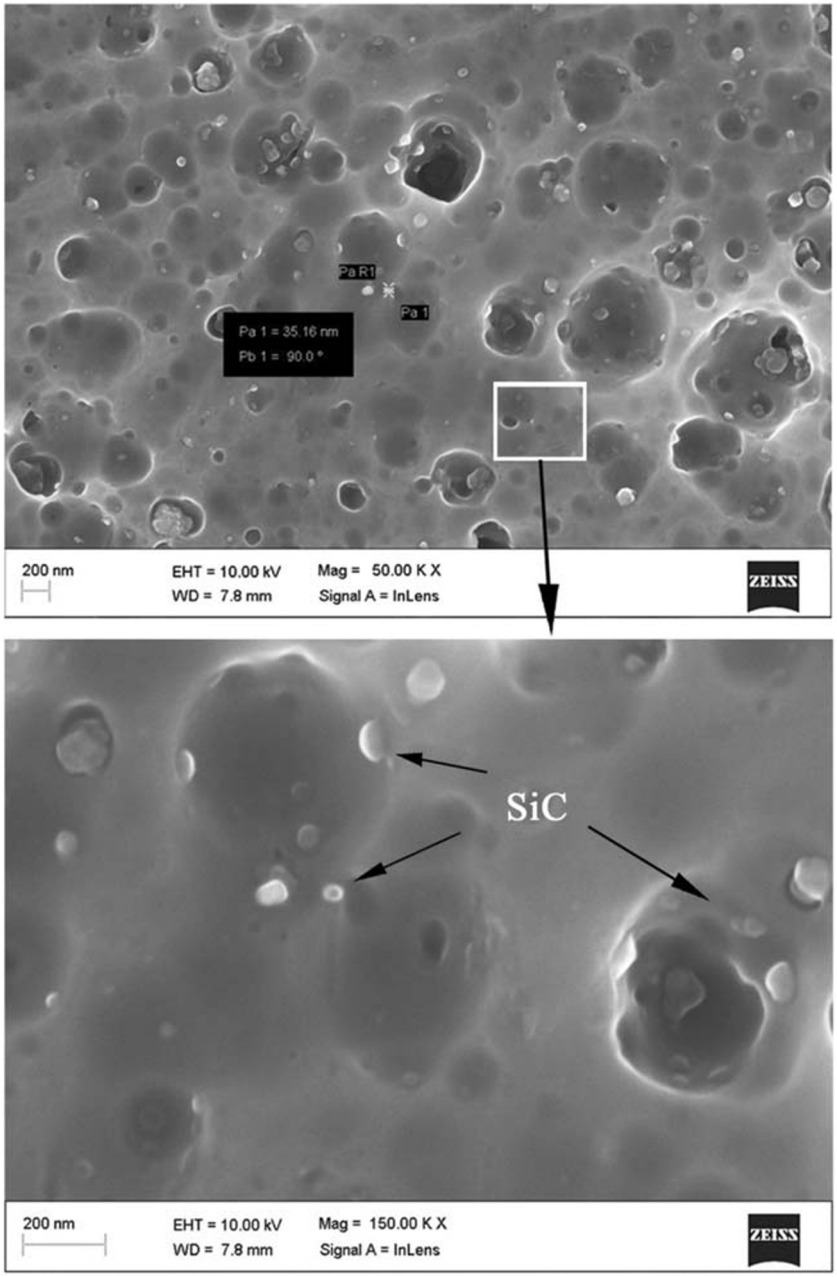

Fig. 8 FESEM micrograph of SZ of SFSSW joint produced under optimal condition

Figure 7 is the micrograph of different regions of the cross-section of weld sample prepared with the optimal process parameters (the guide hole diameter (D) = 3 mm, tool rotational speed (N) = 1600 rpm and the tool traverse speed (F) = 20 mm/min). The onion ring-like structure was observed in SZ as shown in Fig. 7(b), which evidences the optimum stirring during SFSSW. The dark and bright rings in onion ring show the concentric distribution of SiC nanoparticles [36].

The dynamic recrystallization in SZ is observed as shown in Fig.7(c). It evidences the microstructure of fine dynamically recrystallized grains. This is due to high frictional heat and severe plastic deformation during the weld process. It caused stretching of SiC nanoparticles in SZ and resulted the significant grain refinement [35]. Thermo-mechanically affected zone (TMAZ) experiencing plastic deformation at high temperature showed the better grain refinement compared with the base metal (BM). The grain size measured from SZ of nanoparticles-free sample and SiC added sample are 32 μm and 22 μm respectively. Though both samples were welded with the optimized process parameters, the SiC nanoparticles added sample resulted reduced grain size in the weld area.

The FESEM micrograph in the SZ of weld sample produced with the optimal condition is shown in Fig. 8. Most of the SiC nanoparticles were present in the grain boundaries. The excellent coherency between nanoparticles and aluminium matrix is also observed. The grain boundary pinning of

nanoparticles which are responsible for grain refinement is also evidenced [35–37] at higher magnification. Sing et al. [36] unveiled in their study on the AA6061-T6 that, the added Al_2O_3 nanoparticles caused the refinement of grains in the SZ due to the pinning effect on the migration of grain boundaries.

Energy Dispersive X-ray (EDX) analysis of SiC added composite weld joint(prepared under optimal parameters) and the corresponding elemental mapping images are shown in Fig. 9. The distribution of aluminium, silicon, carbon and magnesium elements are visible in Fig. 9(a), which confirms the homogeneous distribution and mixing of SiC nanoparticles in the aluminium matrix. Furthermore, the images show the absence of any interfacial reaction, which is in line with the work reported by Dinaharan et al. [37] for friction stir processing.

3.6 Microhardness of the Sample Prepared under Optimal Condition

The microhardness of SiC nanoparticles added weld samples and neat weld samples was studied. Both of these weld samples were prepared under optimal condition. The

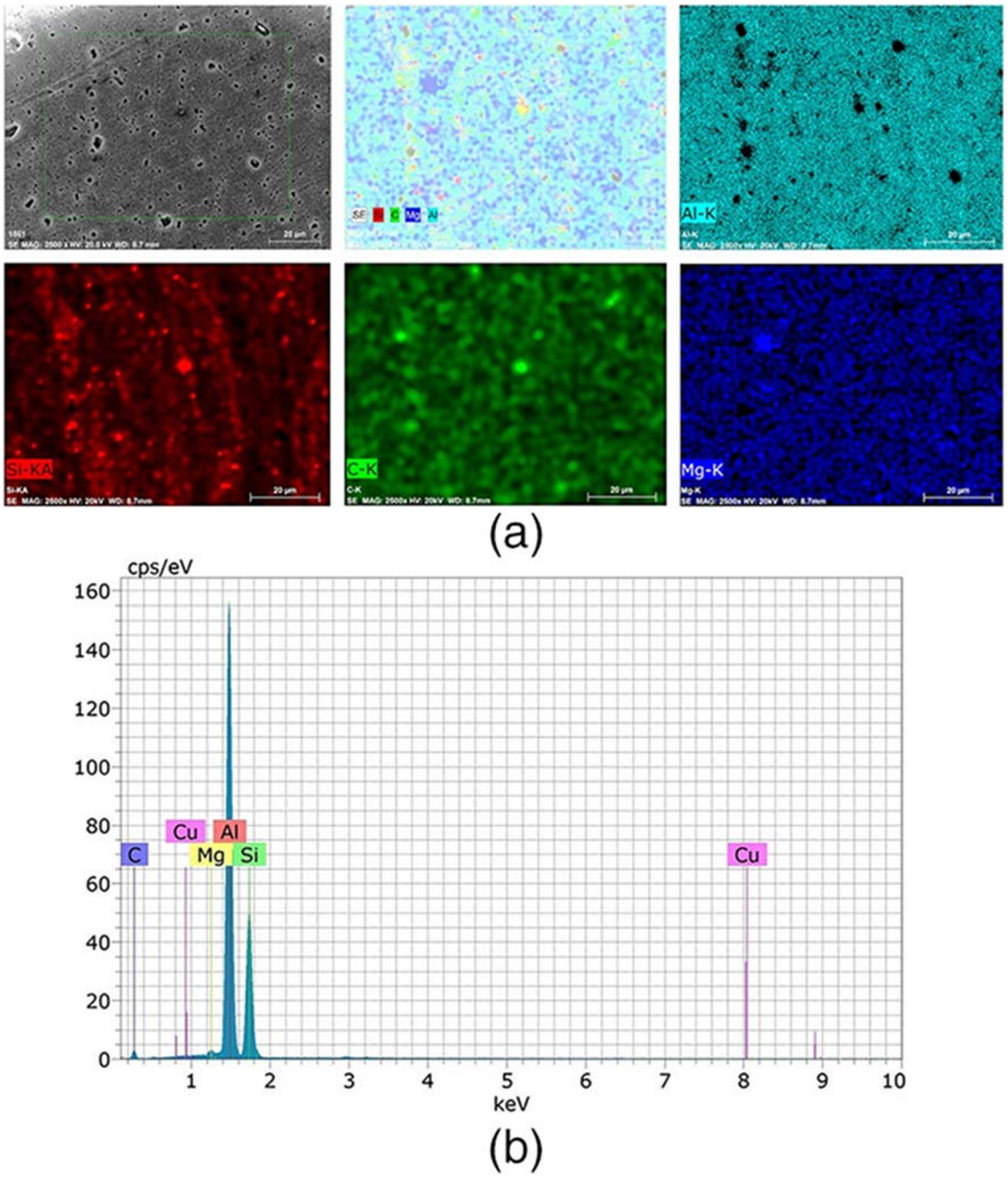

Fig. 9 (**a**) Elemental mapping images and (**b**) EDXprofile of the SZ of the weld joint prepared under optimal condition

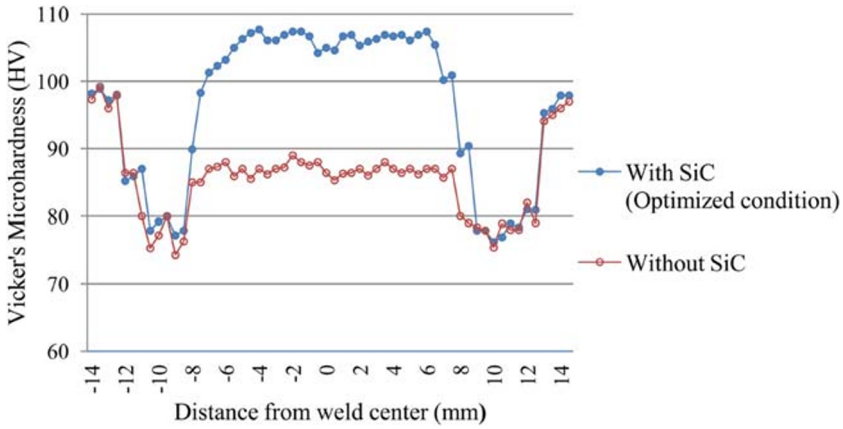

Fig. 10 Microhardness distribution across the weld cross-section (both samples were prepared under optimal condition)

microhardness profile at the lower portion of the keyhole and close to the separation line in the lower plate of the cross-sectioned samples is shown in Fig. 10. The average microhardness at SZ of SiC added weld sample and neat weld samples found to be 105 HV and 84.2 HV respectively. The significant increase of 25% in hardness is observed in SiC added weld sample.

From Fig. 10 it is clear that microhardness values were significantly increased due to addition of SiC nanoparticles into guide hole. It attributed to the grain size and dislocation density and hence increased hardness at SZ. It is also observed from both weld samples, the hardness was decreased in TMAZ and HAZ of both sides. The lower hardness in the HAZ indicates that the failure would start from the respective region and propagate to the other regions as reported by Singh et al. [38].

3.7 Lap Shear Strength of the Sample Prepared under Optimal Condition and its Fracture Morphology

Shear fracture, Plug shear fracture, Plug shear-pullout fractures are different mode of failures observed from the lap shear test specimens. The different mode of failure were observed from the macro images of fracture surfaces of SFSSW joints

Welding condition	Process parameters	Appearance of fracture surfaces			Lap shear strength and fracture type
		Top of top plate	Bottom of top plate	Top of bottom plate	
Exp. no 1	D=1.5 mm N=1200 rpm F=10 mm/min	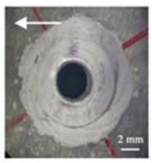	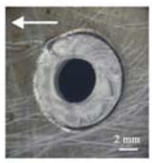	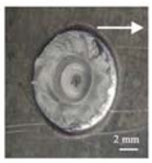	**5740 N** Shear fracture
Exp. no 9	D=2.5 mm N=1200 rpm F=20 mm/min	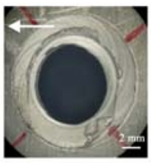	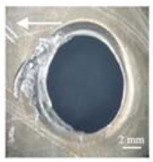	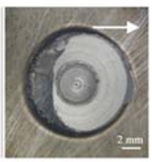	**6456 N** Plug shear fracture
Optimal condition	D=3.0 mm N=1600 rpm F=20 mm/min	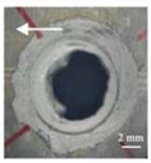	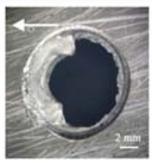	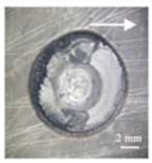	**6790 N** Plug shear - pullout mode fracture
SiC free condition	Without SiC N=1600 rpm F=20 mm/min	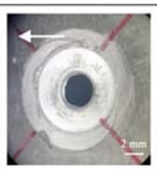	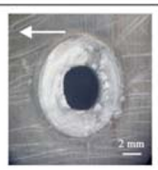	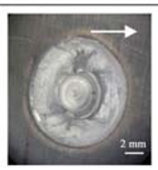	**5623 N** Shear fracture

Fig. 11 Photograph of fracture surfaces after lap shear test at different welding conditions (Arrow marks indicate the direction of loading during lap shear test)

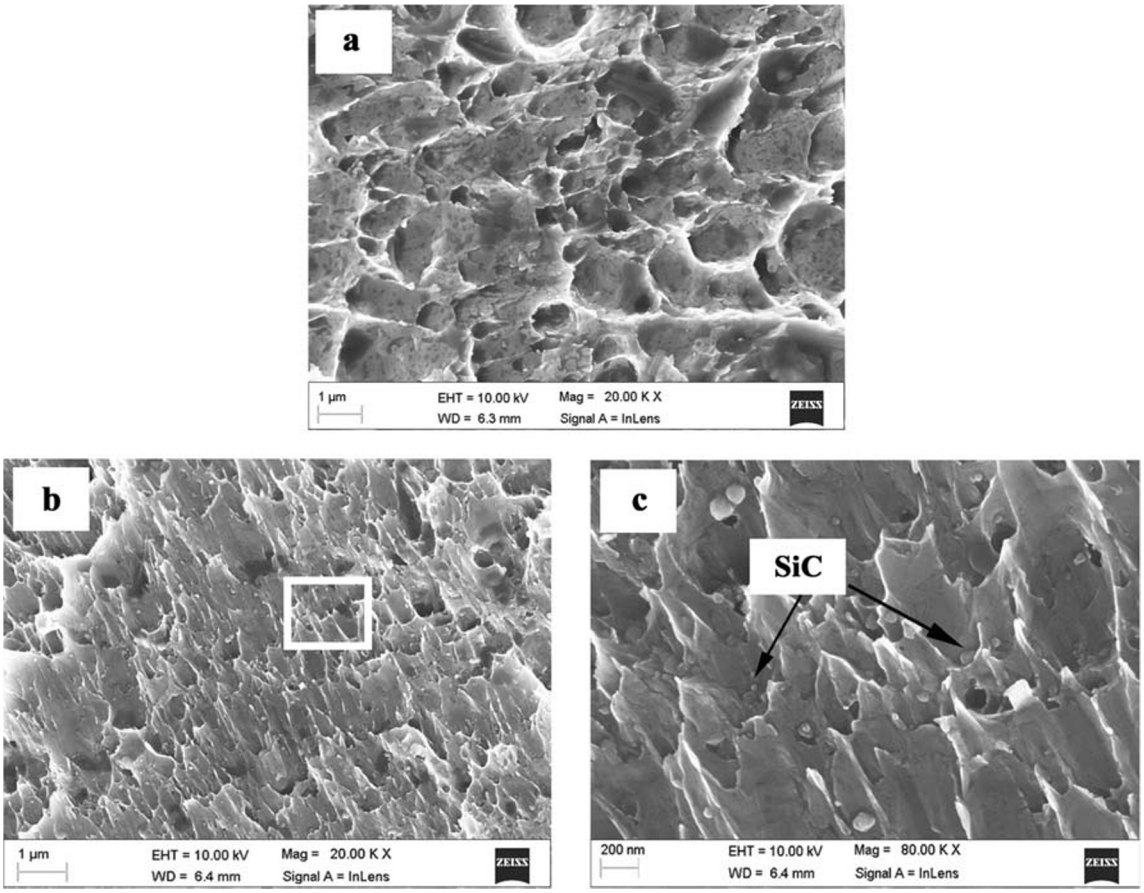

Fig. 12 FESEM fractograph of sample (**a**) Without SiC (**b**) With SiC (optimized condition) and (**c**) magnified view of portion mentioned in (**b**)

prepared at different welding condition as shown in Fig. 11. The samples of the experiment number 1, 2, 4 and 5 experienced shear fracture, samples of experiment number 3, 6, 7, 8, 9, 10, 11 and 13 experienced plug shear fracture, and samples of experiment number 12, 14, 15 and 16 experienced a plug shear-pullout fractures.

The samples that showed shear fracture mode of failure had a low range of lap shear strength as compared to the samples that show other modes of failure. In shear failure mode, the fracture starts in the incompletely bonded region and spread along the boundary between the welded sheets due to tensile loading. This is the reason for resulting lower lap shear strength.

The sample welded under optimal parameters showed the plug shear-pullout mode of fracture. It has lap shear strength of 6790 N which is 21% higher than the SiC free joint produced at the same optimal condition. In this mode, fracture occurred between the two plates in the stir zone and nugget is pulled out from the bottom sheet. The pulled out nugget in the upper sheet indicates the best mechanical bonding between the aluminium material and added nanoparticles. This is the reason for these specimens that failed under plug shear-pullout mode of fracture to have high weld strength than other samples.

Figure 12 shows the FESEM fractographs of fracture surfaces of SiC reinforced weld samples and bare weld samples. The fracture surface of the sample without SiC is covered with broad and deep dimples as shown in Fig. 12(a), while the fracture surface of the SiC added sample has smaller and shallow dimples as shown in Fig. 12(b). The SiC added samples show dimple rupture demonstrating ductile fracture, which results higher tensile strength [39, 40]. SiC nanoparticles are visible in the magnified image as shown in Fig. 12(c). It shows good coherency between SiC nanoparticles and aluminium matrix.

4 Conclusions

Optimization of SFSSW parameters for achieving the best microhardness and lap shear strength on 6061-T6 aluminium alloy was attempted with Taguchi based GRA. The weld samples as per L_{16} array were prepared and the respective microhardness and lap shear strength were measured. The following points were arrived from GRA optimization and microstructure analysis;

- The guide hole diameter (D) = 3 mm, tool rotational speed (N) = 1600 rpm and the tool traverse speed (F) = 20 mm/

min are found to be the best process parameters to obtain the maximum microhardness and lap shear strength.
- The experimental validation of the predicted results of GRA reveals that there is an improvement of 62.46% in grey relational grade between initial and optimal parameters level setting. The very minimal difference of 0.006 is noted between predicted GRA and experimental GRA.
- ANOVA analysis reveals that the amount of nanoparticles added into the guide hole is the most significant parameter for obtaining the best weld joint.
- The reinforcement of SiC nanoparticles into the guide hole improved the microhardness and lap shear strength up to 25% and 21%, respectively. This improvement is attributed by the homogeneous distribution of nanoparticles and the grain refinement in the SZ.
- The weld samples prepared at optimal condition evidenced plug-shear pullout mode of fracture.

These results will help the industries to achieve the best SFSSW on AA6061-T6 alloy with great repeatability.

References

1. Jurgen H (2011) Aluminium in innovative light-weight Car design. Mater Trans 52:818–824. https://doi.org/10.2320/matertrans.L-MZ201132
2. Olea CAW, Roldo L, Strohaecker TR, dos Santos JF (2006) Friction stir welding of precipitate Hardenable Aluminium alloys: a review. Weld World 50:78–87. https://doi.org/10.1007/bf03263464
3. Padhy GK, Wu CS, Gao S (2018) Friction stir based welding and processing technologies - processes, parameters, microstructures and applications: a review. J Mater Sci Technol 34:1–38. https://doi.org/10.1016/j.jmst.2017.11.029
4. Suresh S, Venkatesan K, Rajesh S (2019) Optimization of process parameters for friction stir spot welding of AA6061/Al2O3 by Taguchi method. AIP Conf Proc 2128. https://doi.org/10.1063/1.5117961
5. Addison AC, Robelou AJ (2004) Friction stir spot welding: principal parameters and their effects. Proceedings of the 5th international friction stir welding symposium, Metz, France, 14-16
6. Kalagara S, Muci-Kuchler KH, Arbegast W (2010) Visualization of material flow in a refill friction stir spot welding process using marker materials. SAE Int J Mater Manufact 3:628–651. https://doi.org/10.4271/2010-01-0971
7. Yang XW, Fu T, Li WY (2014) Friction stir spot welding: a review on joint macro and microstructure, property, and process Modelling. Adv Mater Sci Eng 2014:1–11
8. Badrinarayan H, Yang Q, Okamoto K (2011) Effect of weld orientation on static strength and failure mode of friction stir stitch welds in lap-shear specimens of aluminum 6022-T4 sheets. Fatigue Fract Eng Mater Struct 34:908–920. https://doi.org/10.1111/j.1460-2695.2011.01584.x
9. Burford DA, Tweedy BM, Widener CA (2008) Fatigue Crack Growth in Integrally Stiffened Panels Joined Using Friction Stir Welding and Swept Friction Stir Spot Welding. J ASTM Int 5(4). Paper ID JAI101568, 2008
10. Shen Z, Yang X, Yang S, Zhang Z, Yin Y (2014) Microstructure and mechanical properties of friction spot welded 6061-T4 aluminum alloy. Mater Des 54:766–778. https://doi.org/10.1016/j.matdes.2013.08.021
11. Chowdhury SH, Chen DL, Bhole SD, Cao X, Wanjara P (2012) Lap shear strength and fatigue life of friction stir spot welded AZ31 magnesium and 5754 aluminum alloys. Mater Sci Eng A 556:500–509. https://doi.org/10.1016/j.msea.2012.07.019
12. Rao HM, Jordon JB, Barkey ME, Guo YB, Su X, Badarinarayan H (2013) Influence of structural integrity on fatigue behavior of friction stir spot welded AZ31 mg alloy. Mater Sci Eng A 564:369–380. https://doi.org/10.1016/j.msea.2012.11.076
13. Uematsu Y, Kakiuchi T, Tozaki Y, Kojin H (2013) Comparative study of fatigue behaviour in dissimilar Al alloy/steel and mg alloy/steel friction stir spot welds fabricated by scroll grooved tool without probe. Sci Technol Weld Join 17(5):348–356. https://doi.org/10.1179/1362171812Y.0000000014
14. Hossain MAM, Hasan MT, Hong ST, Miles M, Cho HH, Han HN (2013) Friction stir spot welded joints of 409L stainless steels fabricated by a convex shoulder tool. Met Mater Int 19:1243–1250
15. Hovanski Y, Santella ML, Grant GJ (2007) Friction stir spot welding of hot-stamped boron steel. Scr Mater 57(9):873–876. https://doi.org/10.1016/j.scriptamat.2007.06.060
16. Su ZM, He RY, Lin PC, Dong K (2016) Fatigue of alclad AA2024-T3 swept friction stir spot welds in cross-tension specimens. J Mater Process Technol 236:162–175. https://doi.org/10.1016/j.jmatprotec.2016.05.014
17. Su ZM, He RY, Lin PC, Dong K (2014) Fatigue analyses for swept friction stir spot welds in lap-shear specimens of alclad 2024-T3 aluminum sheets. Int J Fatigue 61:129–140. https://doi.org/10.1016/j.ijfatigue.2013.11.021
18. Rathee S, Maheshwari S, Siddiquee AN, Srivastava M (2018) Investigating the effects of SiC particle sizes on microstructural and mechanical properties of AA5059/SiC surface composites during multi-pass FSP. Silicon 11:797–805. https://doi.org/10.1007/s12633-018-9958-1
19. Shojaeefard MH, Akbari M, Khalkhali A, Asadi P (2018) Effect of tool pin profile on distribution of reinforcement particles during friction stir processing of B4C/aluminum composites. Proc Inst Mech Engs Part L: J Mater: Design Appl 232(8):637–651. https://doi.org/10.1177/1464420716642471
20. Dolatkhah A, Golbabaei P, BesharatiGivi MK, Molaiekiya F (2012) Investigating effects of process parameters on microstructural and mechanical properties of Al5052/SiC metal matrix composite fabricated via friction stir processing. Mater Des 37:458–464. https://doi.org/10.1016/j.matdes.2011.09.035
21. Mahmoud ERI, Ikeuchi K, Takahashi M (2008) Fabrication of SiC particle reinforced composite on aluminium surface by friction stir processing. Sci Technol Weld Join 13:607–618. https://doi.org/10.1179/136217108X333327
22. Suresh S, Venkatesan K, Elango N, Nanomater J (2018) Influence of SiC nanoparticle reinforcement on FSS welded 6061-T6 aluminum alloy. J Nanomater 2018:1–10. https://doi.org/10.1155/2018/7031867
23. Wu D, Shen J, Lv L, Wen L, Xie X (2017) Effects of nano-SiC on the FSSW welded AZ31 magnesium alloy joints. Mater Sci Technol 33:998–1003. https://doi.org/10.1080/02670836.2016.1254891
24. Tebyani SF, Dehghani K (2015) Friction stir spot welding of interstitial free steel with incorporating silicon carbide nanopowders. Int J Adv Manuf Tech 79:343–350. https://doi.org/10.1007/s00170-015-6788-9
25. Lee SH, Lee DM, Lee KS (2017) Process optimisation and microstructural evolution of friction stir spot-welded Al6061 joints. Mater Sci Technol 33:719–730. https://doi.org/10.1080/02670836.2016.1230661

26. Karthikeyan R, Balasubramanian V (2010) Predictions of the optimized friction stir spot welding process parameters for joining AA2024 aluminum alloy using RSM. Int J Adv Manuf Technol 51:173–183. https://doi.org/10.1007/s00170-010-2618-2
27. Abbass MK, Hussein SK, Khudhair AA (2016) Optimization of mechanical properties of friction stir spot welded joints for dissimilar aluminum alloys (AA2024-T3 and AA 5754-H114). Arab J Sci Eng 41:4563–4572. https://doi.org/10.1007/s13369-016-2172-9
28. Ojo OO, Taban E (2018) Hybrid multi-response optimization of friction stir spot welds: failure load, effective bonded size and flash volume as responses. Sadhana 43:1–13. https://doi.org/10.1007/s12046-018-0882-2
29. Sindhu D, Thakur L, Chandna P (2018) Multi-objective optimization of rotary ultrasonic machining parameters for quartz glass using Taguchi-Grey relational analysis (GRA). Silicon 11:2033–2044. https://doi.org/10.1007/s12633-018-0019-6
30. Thakur A, Manna A, Samir S (2019) Multi-response optimization of turning parameters during machining of EN-24 steel with SiC Nanofluids based minimum quantity lubrication. Silicon 12:71–85. https://doi.org/10.1007/s12633-019-00102-y
31. Lilly Mercy J, Prakash S, Krishnamoorthy A, Ramesh S, Alex Anand D (2017) Multi response optimisation of mechanical properties in self-healing glass fiber reinforced plastic using grey relational analysis. Measurement 110:344–355. https://doi.org/10.1016/j.measurement.2017.07.013
32. Suresh S, Venkatesan K, Natarajan E, Rajesh S, Hong LW (2019) Evaluating weld properties of conventional and swept friction stir spot welded 6061-T6 aluminium alloy. Mater Express 9:851–860. https://doi.org/10.1166/mex.2019.1584
33. Suresh S, Venkatesan K, Natarajan E, Rajesh S (2020) Influence of tool rotational speed on the properties of friction stir spot welded AA7075-T6/Al_2O_3 composite joint. Mater Today: Proc 27:62–67. https://doi.org/10.1016/j.matpr.2019.08.220
34. Suresh S, Elango N, Venkatesan K, Lim WH, Palanikumar K, Rajesh S (2020) Sustainable friction stir spot welding of 6061-T6 aluminium alloy using improved non-dominated sorting teaching learning algorithm. J Mater Res Technol 9(5):11650–11674. https://doi.org/10.1016/j.jmrt.2020.08.043
35. Yuvanarasimman P, Malayalamurthi R (2017) Studies on fractures of friction stir welded Al matrix SiC-B4C reinforced metal composites. Silicon 10(4):1375–1383. https://doi.org/10.1007/s12633-017-9614-1
36. Singh T, Tiwari SK, Shukla DK (2019) Friction-stir welding of AA6061-T6: the effects of Al_2O_3 nano-particles addition. Results Mater 1:100005. https://doi.org/10.1016/j.rinma.2019.100005
37. Dinaharan I, Sathishkumar R, Murugan N (2016) Effect of ceramic particulate type on microstructure and properties of copper matrix composites synthesized by friction stir processing. J Mater Res Technol 5:302–316. https://doi.org/10.1016/j.jmrt.2016.01.003
38. Singh T, Tiwari SK, Shukla DK (2019) Production of AA6061-T6/Al2O3 reinforced nanocomposite using friction stir welding. Eng Res Express 1(2). https://doi.org/10.1088/2631-8695/ab5e27
39. Srivastava M, Rathee S, Siddiquee AN, Maheshwari S (2018) Investigation on the effects of silicon carbide and cooling medium during multi-pass FSP of Al-mg/SiC surface composites. Silicon 11:2149–2157. https://doi.org/10.1007/s12633-018-0037-4
40. Subramani V, Jayavel B, Sengottuvelu R, Lazar P (2019) Assessment of microstructure and mechanical properties of stir zone seam of friction stir welded magnesium AZ31B through Nano-SiC. Materials 12(7):1044. https://doi.org/10.3390/ma12071044